

Sizes of pure and doped helium droplets from single shot x-ray imaging

Cite as: J. Chem. Phys. **156**, 041102 (2022); <https://doi.org/10.1063/5.0080342>

Submitted: 30 November 2021 • Accepted: 07 January 2022 • Accepted Manuscript Online: 07 January 2022 • Published Online: 31 January 2022

 Rico Mayro P. Tanyag,  Camila Bacellar, Weiwu Pang, et al.



View Online



Export Citation



CrossMark

ARTICLES YOU MAY BE INTERESTED IN

Stronger orientation of state-selected OCS molecules with relative-delay-adjusted nanosecond two-color laser pulses

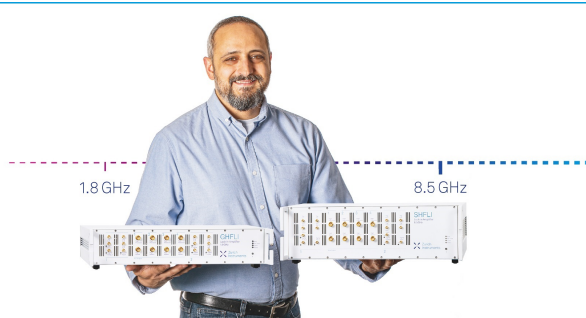
The Journal of Chemical Physics **156**, 041101 (2022); <https://doi.org/10.1063/5.0075849>

Initial state-selected scattering for the reactions $H + CH_4/CHD_3$ and $F + CHD_3$ employing ring polymer molecular dynamics

The Journal of Chemical Physics **156**, 044101 (2022); <https://doi.org/10.1063/5.0076216>


Two-component density functional theory for muonic molecules: Inclusion of the electron-positive muon correlation functional

The Journal of Chemical Physics **156**, 044104 (2022); <https://doi.org/10.1063/5.0077179>



Trailblazers. New

Meet the Lock-in Amplifiers that measure microwaves.

 Zurich Instruments [Find out more](#)

Sizes of pure and doped helium droplets from single shot x-ray imaging

Cite as: J. Chem. Phys. 156, 041102 (2022); doi: 10.1063/5.0080342

Submitted: 30 November 2021 • Accepted: 7 January 2022 •

Published Online: 31 January 2022



Rico Mayro P. Tanyag,^{1,a),b)} Camila Bacellar,^{2,3,c)} Weiwu Pang,⁴ Charles Bernando,^{5,d)} Luis F. Gomez,¹ Curtis F. Jones,^{1,e)} Ken R. Ferguson,⁶ Justin Kwok,^{7,f)} Denis Anielski,⁸ Ali Belkacem,² Rebecca Boll,^{8,g)} John Bozek,⁶ Sebastian Carron,⁶ Gang Chen,^{9,h)} Tjark Delmas,¹⁰ Lars Englert,^{11,i)} Sascha W. Epp,^{8,j)} Benjamin Erk,^{8,k)} Lutz Foucar,¹² Robert Hartmann,¹³ Alexander Hexemer,⁹ Martin Huth,^{13,l)} Stephen R. Leone,^{2,3,14} Jonathan H. Ma,² Stefano Marchesini,⁹ Daniel M. Neumark,^{2,3} Billy K. Poon,^{15,m)} James Prell,^{2,3} Daniel Rolles,^{8,16} Benedikt Rudek,^{8,n)} Artem Rudenko,^{8,16} Martin Seifrid,¹ Michele Swiggers,⁶ Joachim Ullrich,^{8,o)} Fabian Weise,² Petrus Zwart,^{15,l),p)} Christoph Bostedt,^{6,17,18} Oliver Gessner,² and Andrey F. Vilesov^{1,5,a)}

AFFILIATIONS

¹ Department of Chemistry, University of Southern California, Los Angeles, California 90089, USA

² Chemical Sciences Division, Lawrence Berkeley National Laboratory, Berkeley, California 94720, USA

³ Department of Chemistry, University of California Berkeley, Berkeley, California 94720, USA

⁴ Department of Computer Science, University of Southern California, Los Angeles, California 90089, USA

⁵ Department of Physics and Astronomy, University of Southern California, Los Angeles, California 90089, USA

⁶ Linac Coherent Light Source, SLAC National Accelerator Laboratory, Menlo Park, California 94025, USA

⁷ Department of Chemical Engineering and Material Science, University of Southern California, Los Angeles, California 90089, USA

⁸ Max-Planck-Institut für Kernphysik, Saupfercheckweg 1, 69117 Heidelberg, Germany

⁹ Advanced Light Source, Lawrence Berkeley National Laboratory, Berkeley, California 94720, USA

¹⁰ Center for Free-Electron Laser Science (CFEL), Deutsches Elektronen-Synchrotron (DESY), Notkestraße 85, 22607 Hamburg, Germany

¹¹ Max-Planck-Institut für extraterrestrische Physik, Giessenbachstraße, 85741 Garching, Germany

¹² Max-Planck-Institut für Medizinische Forschung, Jahnstrasse 29, 69120 Heidelberg, Germany

¹³ PnSensor GmbH, Otto-Hahn-Ring 6, 81739 München, Germany

¹⁴ Department of Physics, University of California Berkeley, Berkeley, California 94720, USA

¹⁵ Physical Biosciences Division, Lawrence Berkeley National Laboratory, Berkeley, California 94720, USA

¹⁶ J.R. MacDonald Laboratory, Department of Physics, Kansas State University, Manhattan, Kansas 66506, USA

¹⁷ Paul-Scherrer Institute, CH-5232 Villigen PSI, Switzerland

¹⁸ LUXS Laboratory for Ultrafast X-ray Sciences, Institute of Chemical Sciences and Engineering, Ecole Polytechnique Fédérale de Lausanne (EPFL), CH-1015 Lausanne, Switzerland

^{a)} Authors to whom correspondence should be addressed: tanyag@chem.au.dk and vilesov@usc.edu

^{b)} Present address: Department of Chemistry, Aarhus University, 8000 Aarhus C, Denmark.

^{c)} Present address: Paul Scherrer Institute, Villigen 5232, Switzerland.

^{d)} Present address: School of Information Systems, BINUS University, Jl. K.H. Syahdan No. 9, Kemanggisan, Palmerah, Jakarta 11480, Indonesia.

^{e)} Present address: State University of New York (SUNY) Adirondack, Queensbury, NY 12804, USA.

^{f)} Present address: Department of Materials Science and Engineering, University of Illinois at Urbana-Champaign, Urbana, IL 61801, USA.

^{g)} Present address: European XFEL, Holzkoppel 4, 22869 Schenefeld, Germany.

^{h)} Present address: School of Physical Science and Technology, ShanghaiTech University, Shanghai 201210, China.

- ^{j)} **Present address:** Department of Physics, Carl von Ossietzky University Oldenburg, 26129 Oldenburg, Germany.
- ^{j)} **Present address:** Max-Planck-Institut für Struktur und Dynamik der Materie, Luruper Chaussee 149, 22761 Hamburg, Germany.
- ^{k)} **Present address:** Deutsches Elektronen-Synchrotron DESY, 22607 Hamburg, Germany.
- ^{j)} **Present address:** PNDetector GmbH, Otto-Hahn-Ring, 681739 München, Germany.
- ^{m)} **Present address:** Molecular Biophysics and Integrated Bioimaging, Lawrence Berkeley National Laboratory, Berkeley, CA 94720, USA.
- ⁿ⁾ **Present address:** Department of Radiation Oncology, VA Medical Center, Boston, MA 02130, USA.
- ^{o)} **Present address:** Physikalisch-Technische Bundesanstalt, Bundesallee 100, 38116 Braunschweig, Germany.
- ^{p)} **Present address:** Center for Advanced Mathematics in Energy Research Applications, Lawrence Berkeley National Laboratory, Berkeley, CA 94720, USA.

ABSTRACT

Advancements in x-ray free-electron lasers on producing ultrashort, ultrabright, and coherent x-ray pulses enable single-shot imaging of fragile nanostructures, such as superfluid helium droplets. This imaging technique gives unique access to the sizes and shapes of individual droplets. In the past, such droplet characteristics have only been indirectly inferred by ensemble averaging techniques. Here, we report on the size distributions of both pure and doped droplets collected from single-shot x-ray imaging and produced from the free-jet expansion of helium through a 5 μm diameter nozzle at 20 bars and nozzle temperatures ranging from 4.2 to 9 K. This work extends the measurement of large helium nanodroplets containing 10^9 – 10^{11} atoms, which are shown to follow an exponential size distribution. Additionally, we demonstrate that the size distributions of the doped droplets follow those of the pure droplets at the same stagnation condition but with smaller average sizes.

Published under an exclusive license by AIP Publishing. <https://doi.org/10.1063/5.0080342>

I. INTRODUCTION

Superfluid helium droplets are versatile media for many experiments in chemistry and physics.^{1–3} Helium does not have a triple point and only turns solid at pressures greater than 25 bars.⁴ In vacuum, the droplets remain in a liquid state and cool by evaporation to a temperature of ~ 0.4 K,^{5,6} which is below the superfluid transition temperature for liquid helium at 2.17 K.⁴ As individual isolated cryostats, helium droplets are used for high resolution spectroscopy of embedded clusters of atoms and/or molecules and for the assembly of far-from-equilibrium nanostructures.^{1–3} They are also used as a weakly interacting matrix for studying and controlling the orientation and alignment of embedded molecules.^{7–9} In addition, large nanodroplets offer an opportunity for the formation and assembly of large dopant clusters and for investigating size-dependent properties of clusters, such as their optical absorption and catalytic properties.^{10–12} Recently, shape deformations and *in situ* configurations of xenon-traced quantum vortices in rotating, self-contained, and superfluid droplets with sizes ranging from 5×10^7 to 10^{11} atoms were observed using x-ray coherent diffractive imaging (XCDI).^{13–17}

Helium droplets are produced in a cryogenic nozzle beam expansion of helium into vacuum with sizes ranging from 10^3 up to 10^{12} helium atoms, corresponding to diameters between ~ 4.5 nm and ~ 4.5 μm . Size distributions of droplets containing up to about 10^8 atoms have previously been obtained via beam deflection upon pickup of heavy atoms¹⁸ or via electric field deflection of ionized droplets.^{19–26} More recently, the average sizes of droplets with 10^5 – 10^{12} helium atoms were determined using the “titration” technique, which relies on the attenuation of the flux of helium atoms carried by the droplet beam upon multiple collisions with rare gas atoms.²⁷ For large nanodroplets containing $\sim 10^7$ helium atoms, the droplet sizes follow an exponential size distribution.^{19,21,22} The size

distribution of the droplets is a critical experimental parameter and is essential in determining size-dependent effects of droplet properties, such as its superfluidity.²⁸ In addition, the droplet size defines the largest dopant cluster size that can be assembled in the droplet, which is limited by the evaporation of the entire droplet.^{1,29} Finally, in order to characterize size-dependent properties of dopant clusters assembled inside helium droplets, the size distribution of doped droplets must also be considered.

The recent emergence of coherent, intense, and ultrashort extreme ultraviolet (XUV) and soft x-ray light sources, such as High Harmonic Generation (HHG) and Free-Electron Lasers (FELs), has enabled measurements of individual diffraction patterns of pure and doped helium droplets.^{13–15,30,31} The majority of the droplets have spheroidal shape. From the diffraction, the droplet’s semi-major, R_{major} , and semi-minor, R_{minor} , axes are attained rather than the number size, N_{He} , as determined in other techniques; see Refs. 19–27 and 32. In this work, x-ray scattering is used to determine the sizes of individual droplets with nanometer resolution, from which size distributions of both pure and doped helium droplets were obtained. We found that the size distributions are exponential for both pure and doped droplets. The decrement in the average size of doped droplets is in quantitative agreement with the evaporation model and corroborates the accuracy of average droplet sizes obtained using the titration technique, which is grounded on the validity of the exponential distribution but could not be independently verified previously.

II. EXPERIMENTAL SETUP

X-ray diffraction experiments on helium droplets were performed with the CFEL-ASG Multi-Purpose (CAMP) instrument¹⁸ at the atomic, molecular, and optical (AMO) sciences beamline of

the Linac Coherent Light Source (LCLS) at SLAC National Accelerator Laboratory.¹³ Single-shot diffraction images from helium droplets are collected at small scattering angles ($<4^\circ$) with a cooled pn-junction charge-coupled device (pnCCD) detector. The pnCCD detector assembly consists of two plates each having 512×1024 pixels and separated by a ~ 2 mm gap. One square pixel has a side length of $75 \mu\text{m}$.¹⁸ Both plates have a semi-circular cut to allow for the passage of the primary x-ray beam. LCLS was operated with a photon energy of 1.5 keV, a pulse energy of ~ 2 mJ, a pulse duration of ~ 100 fs, a repetition rate of 120 Hz, and a focal spot cross-sectional area of $\sim 25 \mu\text{m}^2$.³³ A more detailed description of the experimental setup was given in Ref. 13.

Helium droplets are produced from the free-jet expansion of high purity (99.9999%) helium into vacuum through a pinhole with a nominal diameter of $5 \mu\text{m}$. The stagnation pressure is maintained at 20 bars, while the nozzle temperature, T_0 , is varied from 4.2 to 9.0 K. The central part of the helium beam expansion passes through a 0.5 mm diameter skimmer. Downstream, the droplets traverse a 10 cm long pick-up cell filled with xenon. Due to the heavier mass of the droplets, the scattering of the beam is negligible.²⁷ When a droplet captures xenon, about 250 helium atoms are evaporated as estimated from the thermal energy and enthalpy of sublimation of xenon.^{27,29} As a result, the droplet size decreases upon capture of multiple xenon atoms, and concomitantly, the flux of helium atoms carried by the droplets also decreases.²⁷ This flux is measured by the partial pressure rise of helium in a mass spectrometer chamber, which is the terminal chamber of the droplet beam setup. The amount of flux attenuation, AT , due to doping is estimated from the helium pressure rise due to the doped droplet beam, P_{He} , and the pressure rise due to the pure droplet beam, $P_{\text{He},0}$, and is given by^{2,27}

$$AT = \left(1 - \frac{P_{\text{He}}}{P_{\text{He},0}}\right). \quad (1)$$

If the initial mean size of the droplets is known, the average number of evaporated helium atoms can be determined, as well as the average number of captured particles per droplet.^{2,27} While attenuation levels up to $AT = 0.98$ were explored, droplet size determination via diffraction was only feasible for $AT \leq 0.7$. At higher levels of doping, the diffraction signal from the residual helium droplets becomes too small for the size determination. Additionally, many of the diffraction images obtained at high levels of xenon doping resemble those obtained for pure xenon clusters measured in Ref. 34.

During the experiments, two nozzles with the same nominal diameter of $5 \mu\text{m}$ were used. At the same stagnation conditions, nozzle A gave sizes comparable to previous titration measurements,²⁷ while nozzle B gave smaller sizes. This effect is likely due to partial clogging of nozzle B. The average sizes of the droplets produced at $T_0 = 5.0$ K, as estimated in this work, using the titration technique are 3×10^{11} for nozzle A and 5×10^8 for nozzle B. We report the sizes determined using the XCDI technique for both nozzles.

III. RESULTS

A. Determination of the droplet size

Diffraction images collected from (a) a pure and (b) a doped droplet are shown in Fig. 1. The diffraction pattern from pure droplets contains concentric circular or elliptical contours, which

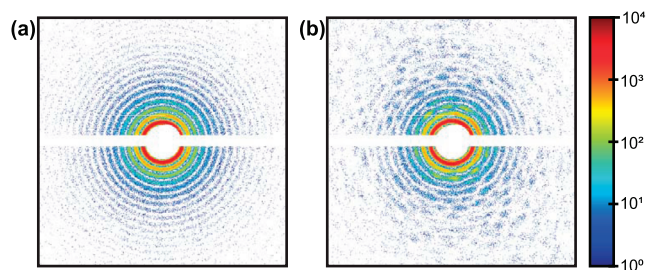


FIG. 1. Examples of diffraction patterns from a pure (a) and a xenon-doped (b) droplet. Colors indicate intensities (in detector units) at each pixel on a logarithmic scale. The images represent the central 512×512 detector pixels. The horizontal stripe in both images results from the gap between the upper and lower detector panels. The hole at the center is to allow for the primary x-ray beam to pass through.

are ascribed to spherical or oblate pseudo-spheroidal droplet shapes, respectively.^{13–15} The details of the droplet size and shape determination from the diffraction scattering patterns are described elsewhere.^{13,14,35} Briefly, the radial intensity profiles in a diffraction image at fixed azimuthal angles are fitted by the square of the Bessel function of order 3/2. Each fit of the Bessel function determines an effective radius. The collection of radii at different azimuthal angles are, then, fitted to an equation of an ellipse, providing the major and minor radii (R_{major} , R_{minor}) and the aspect ratio $AR = R_{\text{major}}/R_{\text{minor}}$ of a droplet. Droplets with radii smaller than ~ 50 nm could not be analyzed in this work due to the diminishing scattering signal. The upper radius limit of ~ 1500 nm is determined by the detector resolution. To fully resolve adjacent diffraction rings, they should be separated by at least three detector pixels. The number size of a pseudo-spheroidal droplet is estimated as

$$N_{\text{He}} = \frac{4\pi \cdot n_{\text{He}}}{3} \cdot R_{\text{major}}^2 \cdot R_{\text{minor}}, \quad (2)$$

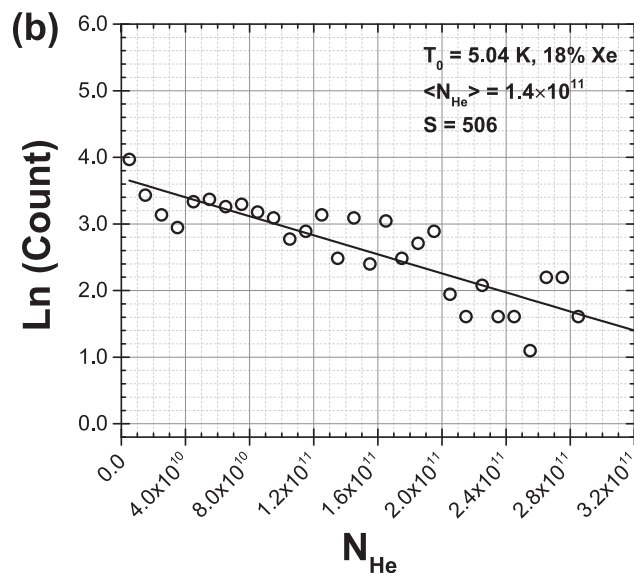
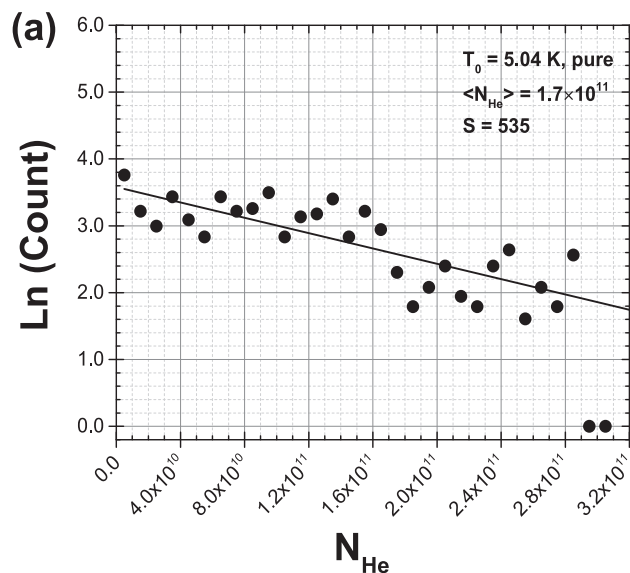
where $n_{\text{He}} = 21.8 \text{ nm}^{-3}$ is the helium number density at low temperatures.³⁶ Because the droplets are imaged at an arbitrary angle with respect to its (minor) figure axis, R_{major} gives the major half-axis of the droplet, while R_{minor} gives an upper boundary of the droplet's minor half-axis.^{13,14} Consequently, Eq. (2) typically overestimates a droplet's actual size. However, 90% of the events correspond to $AR < 1.1$ and using Eq. (2) will only give an overestimation of N_{He} by less than 10% for the average sizes presented in this work. We also ignore prolate-shaped droplets in this work, since they are formed with a probability of $<1.5\%$.^{15,37}

At low to moderate doping levels ($AT = 0.10$ – 0.70), the diffraction patterns contain well-defined concentric rings close to the center of the image, such as in Fig. 1(b). From these rings, which remain discernible up to five rings from the center of a diffraction image, the size and shape of a doped droplet can be accurately determined. The speckles observed away from the center originate from the interference of radiation scattered from the droplet and the embedded dopant clusters and do not affect the measurement of the size of the doped droplet.^{38,39}

B. Average droplet size and size distribution

A total of roughly 12 000 images of pure and doped droplets were obtained in this work. From this number, about 40% were

Nozzle A



Nozzle B

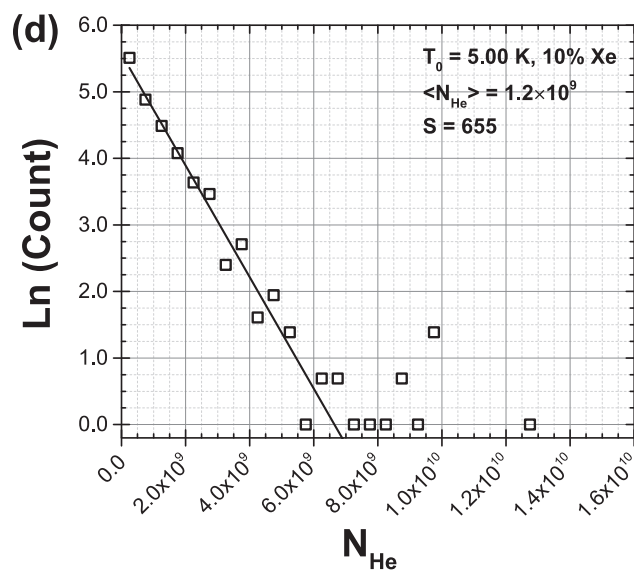
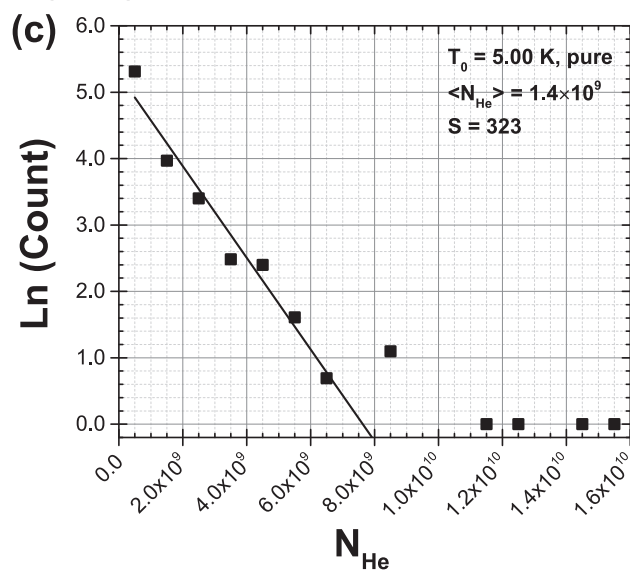


FIG. 2. Size distributions for [(a) and (c)] pure and [(b) and (d)] doped droplets. (a) Droplets were obtained with nozzle A at $T_0 = 5.04$ K. (b) Same nozzle conditions as in (a) but for xenon-doped droplets at $AT = 18\%$. (c) Droplets were obtained with nozzle B at $T_0 = 5.00$ K. (d) Same as in (c) but for xenon-doped droplets at $AT = 10\%$. The solid line in each panel shows a fit in Eq. (3). Bin size is 10^{10} in (a) and (b), 10^9 in (c), and 5×10^8 in (d).

rejected based on a low photon count of <5000 photons per image. Some images are also excluded if the fitted ellipse to the measured radii at different azimuthal angles gave a root mean square deviation larger than 1%.³⁵ Figure 2 shows size distributions for pure [(a) and (c)] and doped [(b) and (d)] droplets at a nozzle temperature of ~ 5 K, which falls within the liquid fragmentation regime of helium droplet production. The droplet sizes in this regime were previously described by an exponential distribution,^{19,22}

$$f(N_{\text{He}}) = \frac{S}{\langle N_{\text{He}} \rangle} \exp\left(-\frac{N_{\text{He}}}{\langle N_{\text{He}} \rangle}\right), \quad (3)$$

where $\langle N_{\text{He}} \rangle$ is the average droplet size and S is the total number of detected droplets. Fitting Eq. (3) to the experimental results shown in Fig. 2 gives the average droplet sizes, $\langle N_{\text{He}} \rangle$. Table I enumerates $\langle N_{\text{He}} \rangle$ obtained from nozzle A at $T_0 = 5.04$ K and nozzle B at $T_0 = 5.00$ K. Additionally, Table I lists the doping levels, given in

TABLE I. Ensemble average sizes, $\overline{N_{\text{He}}}$, and root mean square deviation, σ , of pure and xenon-doped droplets and average droplet sizes, $\langle N_{\text{He}} \rangle$, obtained from the exponential fits; see Eq. (3). The droplets were obtained at the given temperature T_0 and at constant stagnation pressure $P_0 = 20$ bars. The doping level is given in percent attenuation, % AT, and the number of droplets detected at each nozzle stagnation condition is expressed with symbol S.

Nozzle	T_0 (K)	AT (%)	S	$\overline{N_{\text{He}}}$	σ	$\langle N_{\text{He}} \rangle$
A	5.04	0	535	1.1×10^{11}	0.8×10^{11}	1.7×10^{11}
		18	506	1.0×10^{11}	0.8×10^{11}	1.4×10^{11}
		36	532	7.7×10^{10}	6.7×10^{10}	8.1×10^{10}
B	5.00	0	323	1.4×10^9	2.0×10^9	1.4×10^9
		10	655	1.3×10^9	1.6×10^9	1.2×10^9
		27	108	9.4×10^8	9.7×10^8	11.5×10^8
		50	190	4.6×10^8	8.9×10^8	6.4×10^8
		62	61	4.5×10^8	7.9×10^8	4.1×10^8
		67	175	3.5×10^8	6.2×10^8	3.2×10^8

%AT; the number of detected droplets, S; and the ensemble average droplet sizes, $\overline{N_{\text{He}}}$, measured from the diffraction images of individual droplets and their corresponding standard deviation, σ . An expanded version for all other nozzle stagnation conditions explored in this work is given in Table SI of the [supplementary material](#). As can be noted in Table I, there is good agreement between $\overline{N_{\text{He}}}$ and N_{He} for the smaller droplets obtained with nozzle B. For pure droplets produced using nozzle A at $T_0 = 5.04$ K, $\langle N_{\text{He}} \rangle = 1.7 \times 10^{11}$, while $\overline{N_{\text{He}}} = 1.1 \times 10^{11}$. Larger values of $\langle N_{\text{He}} \rangle$ than $\overline{N_{\text{He}}}$ were found because droplet sizes of $N_{\text{He}} > 3.2 \times 10^{11}$ could not be determined, so the distributions in Figs. 2(a) and 2(b) only extend to this value. For pure droplets with nozzle B at $T_0 = 5.00$ K [see Fig. 2(c)], $\langle N_{\text{He}} \rangle = 1.4 \times 10^9$ and $\overline{N_{\text{He}}} = 1.4 \times 10^9$ were obtained, which are identical and are expected for an exponential distribution.

The sizes of xenon-doped droplets, as in Figs. 2(b) and 2(d), also follow exponential distribution but with a steeper slope than those of the pure droplets. While the evaporation of helium atoms upon successive capture of dopants reduces the average droplet sizes, the size distribution of doped droplets remains exponential within the accuracy of the measurements. Exponential distribution is characterized by the standard deviation of $\sigma = \langle N_{\text{He}} \rangle$, and the rather close agreement between $\langle N_{\text{He}} \rangle$ and σ in Table I corroborates that the distributions for pure and doped droplets are exponential in nature.

The values of $\langle N_{\text{He}} \rangle$ for different droplet beam attenuations using nozzle B are plotted in Fig. 3. They follow a linear dependence of the form $\langle N_{\text{He}} \rangle = 1.4 \times 10^9 (1 - 1.1AT)$ as indicated by the dashed line, which is very close to the expected $\langle N_{\text{He}, \text{final}} \rangle = 1.4 \times 10^9 (1 - AT)$. This agreement provides an independent validation of the titration technique used in the determination of the average helium droplet size and the average number of the captured dopants, which is based on measuring the attenuation of the droplet beam intensity by a collision gas.²⁷ It also supports a previous assumption in Ref. 27 that the effect of droplet beam broadening due to momentum transfer upon collisions with the dopant particles can be neglected for the large nanodroplets produced in the liquid fragmentation regime.

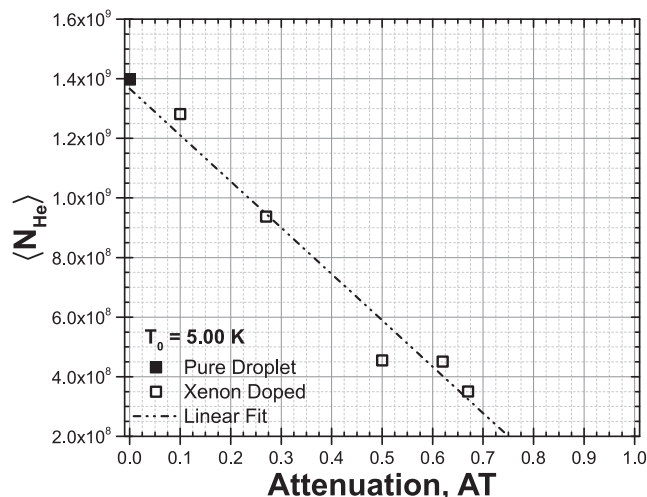


FIG. 3. Average droplets sizes of doped droplets at different attenuation levels with $T_0 = 5.0$ K using nozzle B. The sizes for xenon-doped droplets are shown as open squares, while the filled square indicates the average size of the pure droplets. The dashed line is a linear fit of the droplet sizes at different attenuation levels.

IV. DISCUSSION

The regime of helium droplet production changes based on the state of helium inside the nozzle.^{1,27,40} At constant $P_0 = 20$ bars, the regimes are as follows: (i) condensation of cold helium gas at $T_0 > 10$ K, where the expansion isentropes cross the saturated vapor pressure curve below the critical point ($T_c = 5.2$ K, $P_c = 2.3$ bars); (ii) fragmentation of supercritical fluid at $T_0 = 4$ –10 K; and (iii) breakup of the liquid helium jet at $T_0 < 4$ K.^{1,2} Each regime has its own size distribution and average droplet sizes. Small droplets of about 10^3 – 10^5 atoms, obtained at $T_0 > 10$ K, follow a log-normal distribution.^{32,40} At $T_0 < 4$ K, liquid helium exits the nozzle as a jet that breaks into droplets of almost similar sizes (10^{12} – 10^{13} atoms for a $5 \mu\text{m}$ diameter nozzle) via capillary instability.^{41–43} The nozzle conditions in this work produce the droplets from the fragmentation of liquid helium. In previous studies, droplets with $N_{\text{He}} = 10^5$ – 10^9 were found to follow exponential size distributions.^{21,22,40} One of the salient results of this work extends the validity of the exponential distribution up to $N_{\text{He}} = 10^{11}$.

Average droplet sizes determined from the x-ray diffraction images of pure droplets at different T_0 are plotted in Fig. 4. The results for nozzles A and B are shown as red circles and green diamonds, respectively. The asterisks are the droplet sizes reported in Ref. 27 at the same $P_0 = 20$ bars using the titration technique in a different experimental apparatus. The average sizes obtained with nozzle A at $T_0 = 5$ –6 K are in reasonable agreement with the measurements in Ref. 27. However, the average droplet sizes for nozzle B at $T_0 < 6$ K are a factor of ~ 10 smaller. Droplet production at $T_0 = 5$ K is in the liquid fragmentation regime and proceeds through the rapid boiling and cavitation of liquid helium inside or immediately outside the nozzle.^{27,40} The difference in the average sizes at same T_0 and P_0 for nozzles A and B is likely caused by the perturbation of fluid flow through an obstructed nozzle B. Although working with an obstructed nozzle was not intended, the fact that both noz-

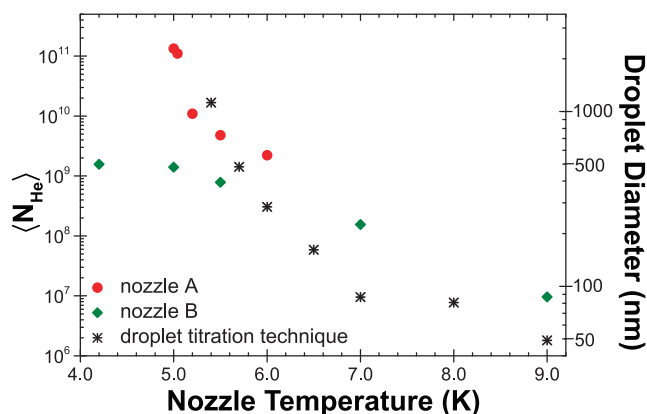


FIG. 4. Average droplet sizes, $\langle N_{\text{He}} \rangle$, vs nozzle temperature, T_0 , at a constant stagnation pressure of 20 bars. The solid shapes represent the average droplet sizes determined in this work using diffraction images from pure droplets. The red circles represent the results obtained using nozzle A, whereas the green diamonds are for nozzle B. The asterisks are the results from Ref. 27 obtained via the titration technique using helium as the collisional gas.

zles A and B produce droplets with exponential distribution is an interesting finding. It shows that the state of the nozzle, which is difficult to control, does not influence obtaining averages, such as $\langle N_{\text{He}} \rangle$, from the titration technique, which implicitly relies on the assumption of the exponential distribution.

At $T_0 > 6$ K, the average droplet sizes observed in this work are approximately ten times larger than previously obtained by titration. This discrepancy may be accounted for by the different nozzle pin-hole plates used and the different beam alignment. In addition, the titration technique underestimates the sizes of small droplets due to droplet beam broadening and deflection as a consequence of collisions with the dopant particles. Likewise, the average droplet size may be overestimated because small droplets may not be reliably detected due to the lower intensity of the x-ray scattering signal.

Previous measurements of the size distribution relied on ionization upon electron impact or electron attachment. Here, the mass-to-charge ratio is typically evaluated by mass spectrometry, where multiple charging of large droplets complicates the interpretation of results.^{21,25,44} Measurements with x-ray scattering can be applied to a range of droplet sizes of about 10^7 – 10^{11} atoms. The lower droplet size boundary for the x-ray parameters used in this experiment is due to the weak scattering signal, whereas the upper boundary is limited by the detector resolution, leading to merging of the diffraction rings. Aside from the weak scattering signal for small droplets, there is also a gradual decrease in their detection probability due to the smaller detection volume for smaller droplets, which is limited to a small portion of the x-ray beam having the largest intensity (see the supplementary material of Ref. 37). For studying the sizes and shapes of much larger droplets, especially those produced in jet breakup, one can use x rays or XUV photons with longer wavelengths or even optical microscopy.

V. CONCLUSIONS

The size distribution of helium droplets is an important experimental parameter that reflects the processes involved in droplet

production. In this paper, we have used a novel technique, single-pulse x-ray coherent diffractive imaging, for the determination of individual droplet sizes. From these, we were able to extract the size distributions of pure and doped droplets. In particular, the distributions of doped droplets were not previously evaluated. Furthermore, the presented measurements extend to the size range of $N_{\text{He}} = 10^9$ – 10^{11} where the validity of exponential size distribution was confirmed. The measurements in this work support the validity of average size determination by the “titration” technique, now widely used in different laboratories for determining average droplet size. In addition, we show that the occurrence of the exponential distribution is insensitive to the state of the nozzle and holds to both the intact and partially obstructed nozzles alike.

SUPPLEMENTARY MATERIAL

See the [supplementary material](#) for the complete tabulation of the measured average droplet sizes at different nozzle stagnation conditions and at a varying xenon doping levels considered in this work and, additionally, the size distribution plots for the conditions reported in [Table I](#).

ACKNOWLEDGMENTS

This work was supported by the NSF under Grant Nos. CHE-1664990 and CHE-2102318 (A.F.V.) and by the U.S. Department of Energy, Office of Basic Energy Sciences (DOE, OBES), Chemical Sciences, Geosciences and Biosciences Division, through Contract Nos. DE-AC02-05CH11231 (C. Bacellar, A.B., O.G., S.R.L., and D.M.N.), DE-AC02-06CH11357 (C. Bostedt), DE-AC02-76SF00515 (C. Bostedt), and DE-FG02-86ER13491 (D.R. and A.R.). We acknowledge the Max Planck Society for funding the development and operation of the CFEL-ASG-Multi-Purpose (CAMP) instrument within the Max Planck Advanced Study Group at the Center of Free-Electron Laser (CFEL) Science. Portions of this research were carried out at the Linac Coherent Light Source, a national user facility operated by Stanford University on behalf of the U.S. DOE, OBES, under beam time Grant No. 2012 SLAC-LCLS AMO54912: Imaging of quantum vortices. We are grateful to James Cryan, Felipe Maia, Erik Malmerberg, Sebastian Schorb, Katrin Siefertmann, and Felix S. Sturm for assisting us during the experiments described in this paper.

AUTHOR DECLARATIONS

Conflict of Interest

The authors have no conflicts to disclose.

DATA AVAILABILITY

The data that support the findings of this study are available from the corresponding authors upon reasonable request.

REFERENCES

- ¹J. P. Toennies and A. F. Vilesov, “Superfluid helium droplets: A uniquely cold nanomatrix for molecules and molecular complexes,” *Angew. Chem., Int. Ed.* **43**(20), 2622–2648 (2004).
- ²R. M. P. Tanyag, C. F. Jones, C. Bernando, S. M. O. O’Connell, D. Verma, and A. F. Vilesov, “Experiments with large superfluid helium nanodroplets,” in *Cold*

Chemistry: Molecular Scattering and Reactivity Near Absolute Zero, edited by O. Dulieu and A. Osterwalder (The Royal Society of Chemistry, London, UK, 2018), pp. 389–443.

- ³A. Mauracher, O. Echt, A. M. Ellis, S. Yang, D. K. Bohme, J. Postler, A. Kaiser, S. Denifl, and P. Scheier, “Cold physics and chemistry: Collisions, ionization and reactions inside helium nanodroplets close to zero K,” *Phys. Rep.* **751**, 1–90 (2018).
- ⁴D. R. Tilley and J. Tilley, *Superfluidity and Superconductivity* (Institute of Physics Publishing, Bristol, 1990).
- ⁵D. M. Brink and S. Stringari, “Density of states and evaporation rate of helium clusters,” *Z. Phys. D: At., Mol. Clusters* **15**(3), 257–263 (1990).
- ⁶M. Hartmann, R. E. Miller, J. P. Toennies, and A. Vilesov, “Rotationally resolved spectroscopy of SF₆ in liquid-helium clusters: A molecular probe of cluster temperature,” *Phys. Rev. Lett.* **75**(8), 1566–1569 (1995).
- ⁷K. Nauta, D. T. Moore, and R. E. Miller, “Molecular orientation in superfluid liquid helium droplets: High resolution infrared spectroscopy as a probe of solvent–solute interactions,” *Faraday Discuss.* **113**, 261–278 (1999).
- ⁸A. S. Chatterley, B. Shepperson, and H. Stapelfeldt, “Three-dimensional molecular alignment inside helium nanodroplets,” *Phys. Rev. Lett.* **119**(7), 073202 (2017).
- ⁹J. W. Niman, B. S. Kaminer, D. J. Merthe, L. Kranabetter, and V. V. Kresin, “Oriented polar molecules trapped in cold helium nanodroplets: Electrostatic deflection, size separation, and charge migration,” *Phys. Rev. Lett.* **123**(4), 043203 (2019).
- ¹⁰J. Tiggesbäumker and F. Stienkemeier, “Formation and properties of metal clusters isolated in helium droplets,” *Phys. Chem. Chem. Phys.* **9**(34), 4748–4770 (2007).
- ¹¹E. Loginov, L. F. Gomez, N. Chiang, A. Halder, N. Guggemos, V. V. Kresin, and A. F. Vilesov, “Photoabsorption of Ag_N (N ~ 6–6000) nanoclusters formed in helium droplets: Transition from compact to multicenter aggregation,” *Phys. Rev. Lett.* **106**(23), 233401 (2011).
- ¹²P. Thaler, A. Volk, D. Knez, F. Lackner, G. Haberfehlner, J. Steurer, M. Schnedlitz, and W. E. Ernst, “Synthesis of nanoparticles in helium droplets—A characterization comparing mass-spectra and electron microscopy data,” *J. Chem. Phys.* **143**(13), 134201 (2015).
- ¹³L. F. Gomez, K. R. Ferguson, J. P. Cryan, C. Bacellar, R. M. P. Tanyag, C. Jones, S. Schorb, D. Anielski, A. Belkacem, C. Bernando, R. Boll, J. Bozek, S. Carron, G. Chen, T. Delmas, L. Englert, S. W. Epp, B. Erk, L. Foucar, R. Hartmann, A. Hexemer, M. Huth, J. Kwok, S. R. Leone, J. H. S. Ma, F. R. N. C. Maia, E. Malmerberg, S. Marchesini, D. M. Neumark, B. Poon, J. Prell, D. Rolles, B. Rudek, A. Rudenko, M. Seifrid, K. R. Siefertmann, F. P. Sturm, M. Swiggers, J. Ullrich, F. Weise, P. Zwart, C. Bostedt, O. Gessner, and A. F. Vilesov, “Shapes and vorticities of superfluid helium nanodroplets,” *Science* **345**(6199), 906–909 (2014).
- ¹⁴C. Bernando, R. M. P. Tanyag, C. Jones, C. Bacellar, M. Bucher, K. R. Ferguson, D. Rupp, M. P. Ziemkiewicz, L. F. Gomez, A. S. Chatterley, T. Gorkhover, M. Muller, J. Bozek, S. Carron, J. Kwok, S. L. Butler, T. Möller, C. Bostedt, O. Gessner, and A. F. Vilesov, “Shapes of rotating superfluid helium nano-droplets,” *Phys. Rev. B* **95**(6), 064510 (2017).
- ¹⁵B. Langbehn, K. Sander, Y. Ovcharenko, C. Peltz, A. Clark, M. Coreno, R. Cucini, M. Drabbs, P. Finetti, M. Di Fraia, L. Giannessi, C. Grazioli, D. Iablonskyi, A. C. LaForge, T. Nishiyama, V. Oliver Álvarez de Lara, P. Piseri, O. Plekan, K. Ueda, J. Zimmermann, K. C. Prince, F. Stienkemeier, C. Allegari, T. Fennel, D. Rupp, and T. Möller, “Three-dimensional shapes of spinning helium nanodroplets,” *Phys. Rev. Lett.* **121**(25), 255301 (2018).
- ¹⁶S. M. O. O’Connell, R. M. P. Tanyag, D. Verma, C. Bernando, W. Pang, C. Bacellar, C. A. Saladrigas, J. Mahl, B. W. Toulson, Y. Kumagai, P. Walter, F. Ancilotto, M. Barranco, M. Pi, C. Bostedt, O. Gessner, and A. F. Vilesov, “Angular momentum in rotating superfluid droplets,” *Phys. Rev. Lett.* **124**(21), 215301 (2020).
- ¹⁷A. J. Feinberg, D. Verma, S. M. O. O’Connell-Lopez, S. Erukala, R. M. P. Tanyag, W. Pang, C. A. Saladrigas, B. W. Toulson, M. Borgwardt, N. Shivaram, M. F. Lin, A. Al Haddad, W. Jäger, C. Bostedt, P. Walter, O. Gessner, and A. F. Vilesov, “Aggregation of solutes in bosonic versus fermionic quantum fluids,” *Sci. Adv.* **7**(50), eabk2247 (2021).
- ¹⁸L. Strüder, S. Eppa, D. Rolles, R. Hartmann, P. Holl, G. Lutz, H. Soltau, R. Eckart, C. Reich, K. Heinzinger, C. Thamm, A. Rudenko, F. Krasniqi, K. U. Kühnel, C. Bauer, C. D. Schroter, R. Moshhammer, S. Techert, D. Miessner, M. Porro, O. Halker, N. Meidinger, N. Kimmel, R. Andritschke, F. Schopper, G. Weiden-spöntner, A. Ziegler, D. Pietschner, S. Herrmann, U. Pietsch, A. Walenta, W. Leitenberger, C. Bostedt, T. Möller, D. Rupp, M. Adolph, H. Graafsma, H. Hirsemann, K. Gartner, R. Richter, L. Foucar, R. L. Shoeman, I. Schlichting, and J. Ullrich, “Large-format, high-speed, X-ray pnCCDs combined with electron and ion imaging spectrometers in a multipurpose chamber for experiments at 4th generation light sources,” *Nucl. Instrum. Methods Phys. Res., Sect. A* **614**(3), 483–496 (2010).
- ¹⁹T. Jiang and J. A. Northby, “Fragmentation clusters formed in supercritical expansions of “He,” *Phys. Rev. Lett.* **68**(17), 2620–2623 (1992).
- ²⁰M. Fárník, U. Henne, B. Samelin, and J. P. Toennies, “Comparison between positive and negative charging of helium droplets,” *Z. Phys. D: At., Mol. Clusters* **40**(1–4), 93–98 (1997).
- ²¹U. Henne and J. P. Toennies, “Electron capture by large helium droplets,” *J. Chem. Phys.* **108**(22), 9327–9338 (1998).
- ²²E. L. Knuth and U. Henne, “Average size and size distribution of large droplets produced in a free-jet expansion of a liquid,” *J. Chem. Phys.* **110**(5), 2664–2668 (1999).
- ²³O. Kornilov and J. R. Toennies, “The determination of the mean sizes of large He droplets by electron impact induced attenuation,” *Int. J. Mass Spectrom.* **280**(1–3), 209–212 (2009).
- ²⁴R. Sliter, L. F. Gomez, J. Kwok, and A. Vilesov, “Size distributions of large He droplets,” *Chem. Phys. Lett.* **600**, 29–33 (2014).
- ²⁵F. Laimer, L. Kranabetter, L. Tiefenthaler, S. Albertini, F. Zappa, A. M. Ellis, M. Gatchell, and P. Scheier, “Highly charged droplets of superfluid helium,” *Phys. Rev. Lett.* **123**(16), 165301 (2019).
- ²⁶F. Laimer, F. Zappa, P. Scheier, and M. Gatchell, “Multiply charged helium droplet anions,” *Chem. - Eur. J.* **27**(25), 7283–7287 (2021).
- ²⁷L. F. Gomez, E. Loginov, R. Sliter, and A. F. Vilesov, “Size of large He droplets,” *J. Chem. Phys.* **135**(15), 154201 (2011).
- ²⁸J. P. Toennies, “Helium clusters and droplets: Microscopic superfluidity and other quantum effects,” *Mol. Phys.* **111**(12–13), 1879–1891 (2013).
- ²⁹M. Lewerenz, B. Schilling, and J. P. Toennies, “Successive capture and coagulation of atoms and molecules to small clusters in large liquid-helium clusters,” *J. Chem. Phys.* **102**(20), 8191–8207 (1995).
- ³⁰D. Rupp, N. Monserud, B. Langbehn, M. Sauppe, J. Zimmermann, Y. Ovcharenko, T. Möller, F. Frassetto, L. Poletto, A. Trabattini, F. Calegari, M. Nisoli, K. Sander, C. Peltz, M. J. Vrakking, T. Fennel, and A. Rouzée, “Coherent diffractive imaging of single helium nanodroplets with a high harmonic generation source,” *Nat. Commun.* **8**, 493 (2017).
- ³¹O. Gessner and A. F. Vilesov, “Imaging quantum vortices in superfluid helium droplets,” *Annu. Rev. Phys. Chem.* **70**, 173–198 (2019).
- ³²M. Lewerenz, B. Schilling, and J. P. Toennies, “A new scattering deflection method for determining and selecting the sizes of large liquid clusters of “He,” *Chem. Phys. Lett.* **206**(1–4), 381–387 (1993).
- ³³P. Emma, R. Akre, J. Arthur, R. Bionta, C. Bostedt, J. Bozek, A. Brachmann, P. Bucksbaum, R. Coffee, F.-J. Decker, Y. Ding, D. Dowell, S. Edstrom, A. Fisher, J. Frisch, S. Gilevich, J. Hastings, G. Hays, P. Hering, Z. Huang, R. Iverson, H. Loos, M. Messerschmidt, A. Miahnahri, S. Moeller, H.-D. Nuhn, G. Pile, D. Ratner, J. Rzepiela, D. Schultz, T. Smith, P. Stefan, H. Tompkins, J. Turner, J. Welch, W. White, J. Wu, G. Yocky, and J. Galayda, “First lasing and operation of an ångström-wavelength free-electron laser,” *Nat. Photonics* **4**(9), 641–647 (2010).
- ³⁴D. Rupp, M. Adolph, L. Flückiger, T. Gorkhover, J. P. Müller, M. Müller, M. Sauppe, D. Wolter, S. Schorb, R. Treusch, C. Bostedt, and T. Möller, “Generation and structure of extremely large clusters in pulsed jets,” *J. Chem. Phys.* **141**(4), 044306 (2014).
- ³⁵R. M. P. Tanyag, Ph.D. thesis, University of Southern California, 2018.
- ³⁶R. J. Donnelly and C. F. Barenghi, “The observed properties of liquid helium at the saturated vapor pressure,” *J. Phys. Chem. Ref. Data* **27**(6), 1217–1274 (1998).

- ³⁷D. Verma, S. M. O. O'Connell, A. J. Feinberg, S. Erukala, R. M. P. Tanyag, C. Bernando, W. W. Pang, C. A. Saladrigas, B. W. Toulson, M. Borgwardt, N. Shivaram, M. F. Lin, A. Al Haddad, W. Jager, C. Bostedt, P. Walter, O. Gessner, and A. F. Vilesov, "Shapes of rotating normal fluid ^3He versus superfluid ^4He droplets in molecular beams," *Phys. Rev. B* **102**(1), 014504 (2020).
- ³⁸R. M. P. Tanyag, C. Bernando, C. F. Jones, C. Bacellar, K. R. Ferguson, D. Anielski, R. Boll, S. Carron, J. P. Cryan, L. Englert, S. W. Epp, B. Erk, L. Foucar, L. F. Gomez, R. Hartmann, D. M. Neumark, D. Rolles, B. Rudek, A. Rudenko, K. R. Siefermann, J. Ullrich, F. Weise, C. Bostedt, O. Gessner, and A. F. Vilesov, "Communication: X-ray coherent diffractive imaging by immersion in nanodroplets," *Struct. Dyn.* **2**(5), 051102 (2015).
- ³⁹C. F. Jones, C. Bernando, R. M. P. Tanyag, C. Bacellar, K. R. Ferguson, L. F. Gomez, D. Anielski, A. Belkacem, R. Boll, J. Bozek, S. Carron, J. Cryan, L. Englert, S. W. Epp, B. Erk, L. Foucar, R. Hartmann, D. M. Neumark, D. Rolles, A. Rudenko, K. R. Siefermann, F. Weise, B. Rudek, F. P. Sturm, J. Ullrich, C. Bostedt, O. Gessner, and A. F. Vilesov, "Coupled motion of Xe clusters and quantum vortices in He nanodroplets," *Phys. Rev. B* **93**(18), 180510 (2016).
- ⁴⁰H. Buchenau, E. L. Knuth, J. Northby, J. P. Toennies, and C. Winkler, "Mass-spectra and time-of-flight distributions of helium cluster beams," *J. Chem. Phys.* **92**(11), 6875–6889 (1990).
- ⁴¹R. E. Grisenti and J. P. Toennies, "Cryogenic microjet source for orthotropic beams of ultralarge superfluid helium droplets," *Phys. Rev. Lett.* **90**(23), 234501 (2003).
- ⁴²R. M. P. Tanyag, A. J. Feinberg, S. M. O. O'Connell, and A. F. Vilesov, "Disintegration of diminutive liquid helium jets in vacuum," *J. Chem. Phys.* **152**(23), 234306 (2020).
- ⁴³K. Kolatzki, M. L. Schubert, A. Ulmer, T. Möller, D. Rupp, and R. M. P. Tanyag, "Micrometer-sized droplets from liquid helium jets at low stagnation pressures," *Phys. Fluids* **34**(1), 012002 (2022).
- ⁴⁴J. A. Northby, "Experimental studies of helium droplets," *J. Chem. Phys.* **115**(22), 10065–10077 (2001).